

# The space group classification of topological band-insulators

Robert-Jan Slager<sup>1</sup>, Andrej Mesaros<sup>2</sup>, Vladimir Juričić<sup>1\*</sup> and Jan Zaanen<sup>1</sup>

**Topological band-insulators (TBIs) are bulk insulating materials, which in the presence of time-reversal symmetry feature topologically protected metallic states on their surface or edge. They have recently been discovered in two- and three-dimensional materials with a strong spin-orbit coupling. These unusual states of quantum matter may host Majorana fermions and provide the condensed-matter realization of the exotic theta-vacuum. The existing classification of TBIs departs from time-reversal symmetry, but the role of the crystal-lattice symmetries in the physics of these topological states has remained elusive. Here we provide the classification of TBIs protected not only by time-reversal, but also by crystalline symmetries. We find three broad classes of topological states:  $\Gamma$  states robust against general time-reversal invariant perturbations; translationally active states protected from elastic scattering, but susceptible to topological crystalline disorder; valley topological insulators sensitive to the effects of non-topological and crystalline disorder. These three classes give rise to 18 different two-dimensional, and, at least 70 three-dimensional TBIs, opening up a route for the systematic search for new types of TBIs.**

Topological phases of free fermionic matter are in general characterized by an insulating gap in the bulk and protected gapless modes on the boundary of the system<sup>1,2</sup>. Integer quantum Hall states represent the first examples of topologically protected phases in the absence of any symmetries, with the topological invariant directly related to the measured Hall conductance<sup>3</sup>. Recently, it has become understood that even in the presence of fundamental symmetries such as time-reversal, topologically protected states of matter can, in principle, exist. In particular, it has been shown that time-reversal invariant (TRI) insulators in two dimensions<sup>4</sup> (2D) and three dimensions (3D; refs 5–7) are characterized by  $Z_2$  topological invariants, which pertain to the existence of the gapless boundary modes robust against time-reversal preserving perturbations, and may host Majorana quasiparticles<sup>8</sup>, as well as provide the condensed-matter realization of the theta-vacuum<sup>9</sup>. The theoretical prediction<sup>10,11</sup> and experimental realization of the  $Z_2$ -invariant topological band insulators<sup>12–16</sup> gave a crucial boost to the understanding of these exotic phases of matter, which culminated in the general classification of topological insulators and superconductors based on time-reversal symmetry (TRS) and particle-hole symmetry within the so-called ten-fold periodic table<sup>17–19</sup>.

The role of the crystal lattice in this classification is to provide a unit cell in the momentum space, the Brillouin zone, topologically equivalent to the  $d$ -dimensional torus, over which the electronic Bloch wavefunctions are defined. The ten-fold classification follows then assuming that all the unitary symmetries of the corresponding Bloch Hamiltonian have been exhausted and therefore the only remaining symmetries are, according to Wigner's theorem, antiunitary TRS and particle-hole symmetry. In 3D, however, by considering a  $Z_2$  TBI as a stack of 2D ones, thus assuming a layered 3D lattice, three additional 'weak' invariants associated with the discrete translation symmetry have been found<sup>5</sup>, which characterize these states, and may be probed by lattice dislocations<sup>20</sup>. On the other hand, it has been realized that topological states protected just

by lattice symmetries, such as inversion, can exist in 3D (refs 21–26). Furthermore, it has been recently found that a state protected both by TRS and the lattice  $C_4$  rotational symmetry susceptible to the lattice dislocations can be possible in 2D (ref. 27). However, in general, the role of the space group symmetries in the physics of topological states remained elusive.

We here provide the complete classification of TBIs protected not only by TRS, but also by space group lattice symmetries. As a starting point, we depart from the construction by Fu and Kane<sup>6,7,21</sup> to compute the  $Z_2$  invariant in terms of the matrix of overlaps

$$w_{mn} = \langle u_m(-\mathbf{k}) | \vartheta | u_n(\mathbf{k}) \rangle \quad (1)$$

where  $\vartheta$  is the time-reversal operator and  $|u_n(\mathbf{k})\rangle$  is the  $n$ th occupied Bloch wavefunction. The quantities of central significance are

$$\delta_i = \frac{\sqrt{\det[w(\Gamma_i)]}}{\text{Pf}[w(\Gamma_i)]} \quad (2)$$

defined at the points  $\Gamma_i$  in the Brillouin zone where the Hamiltonian commutes with the time-reversal operator. Because the matrix  $w$  is antisymmetric at the points  $\Gamma_i$ , the Pfaffian is defined at these points and  $\det[w(\Gamma_i)] = (\text{Pf}[w(\Gamma_i)])^2$ . The topological  $Z_2$  invariant,  $\nu$ , is then given by  $(-1)^\nu = \prod_{\Gamma_i} \delta_i$ , and its non-triviality implies a topological obstruction for defining the wavefunctions through the entire Brillouin zone with an even number of band inversions. Notice that the evaluation of the topological invariant in terms of the signs of the Pfaffian does not depend on the dimensionality but only on the fact that the Hamiltonian possesses TRS which, owing to the vanishing of the Chern number, guarantees the existence of globally defined wavefunctions throughout the Brillouin zone.

First, notice that the set of the points  $\Gamma_i$  at which the Hamiltonian commutes with the time-reversal operator is fixed by the space group of the lattice, see Table 1. Second, we choose the overall phase of the Bloch wavefunctions so that a unique phase, which we dub

<sup>1</sup>Instituut-Lorentz for Theoretical Physics, Universiteit Leiden, PO Box 9506, 2300 RA Leiden, The Netherlands, <sup>2</sup>Department of Physics, Boston College, Chestnut Hill, Massachusetts 02467, USA. \*e-mail: juricic@lorentz.leidenuniv.nl.

**Table 1 | Table of the topological phases in 2D.**

Bravais lattice (PG)	WpG	$\Gamma_i$	$\delta_i$	Index (phase)
Square ( $D_4$ )	$p4mm$	$(\Gamma, M, X, Y)$	$(-1, 1, 1)$	$T-p4mm$ ( $\Gamma$ )
	$p4gm$		$(1, -1, 1)$	$T-p4$ (M)
	$p4$		$(1, 1, -1)$	$p4$ (X–Y-valley)
Rectangular ( $D_2$ )	$p2mm$	$(\Gamma, M, X, Y)$	$(-1, 1, 1)$	$T-p2mm$ ( $\Gamma$ )
	$p2mg$		$(1, -1, 1)$	$T-p2m_M$ (M)
	$p2gg$		$(1, 1, -1)$	$T-p2m_X$ (X)
	$pm, pg$		$(1, 1, 1, -1)$	$T-p2m_Y$ (Y)
Rhombic ( $D_2$ )	$c2mm$	$(\Gamma, M_0, M_{-1}, M_1)$	$(-1, 1, 1)$	$T-c2mm$ ( $\Gamma$ )
	$cm$		$(1, -1, 1)$	$T-c2m$ ( $M_0$ )
			$(1, 1, -1)$	$c2m$ (M–valley)
Oblique ( $C_2$ )	$p2$	$(\Gamma, M_0, M_{-1}, M_1)$	$(-1, 1, 1)$	$T-p2$ ( $\Gamma$ )
	$p1$		$(1, -1, 1)$	$T-p2_{M_0}$ ( $M_0$ )
			$(1, 1, -1)$	$T-p2_{M_{-1}}$ ( $M_{-1}$ )
			$(1, 1, 1, -1)$	$T-p2_{M_1}$ ( $M_1$ )
Hexagonal (hexagonal– $D_6$ )	$p6mm$	$(\Gamma, M_0, M_{-1}, M_1, K_-, K_+)$	$(-1, 1, 1, 1, 1)$	$T-p6mm$ ( $\Gamma$ )
	$p6$		$(1, -1, -1, -1, 1)$	$T-p6$ (M)
			$(1, 1, 1, 1, -1)$	$p6$ (K–valley)
Hexagonal (rhombohedral– $D_3$ )	$p3m1$	$(\Gamma, M_0, M_{-1}, M_1)$	$(-1, 1, 1)$	$T-p3m1$ ( $\Gamma$ )
	$p31m, p3$			

For each of the lattice structures, the corresponding point-group (PG) symmetry and the relevant wallpaper group (WpG), that is, space group, are given. The corners of the square and rectangle are denoted by M, whereas in the triangular Bravais structure they are labelled by K. Additionally, the centres of the edges are denoted by X and Y in both the square and rectangular case and by M in the other lattices<sup>33</sup>. The resulting phases are characterized by the distribution of the  $\delta_i$  at the  $\Gamma_i$  points consistent with the WpG symmetry. Phases cluster in Bravais lattices, with the hexagonal structure being the only exception. In this case the WpGs containing six-fold and three-fold rotational symmetries relate the high-symmetry points in different ways. As a result, the Hamiltonian does not commute with the time-reversal operator at the K points in the latter case. The obtained phases are ultimately protected by TRS (whenever  $\nu = 1$ ), WpG symmetry, or both, and are accordingly indexed. The index (last column) describes the part of the wallpaper group that leaves the subset  $\Gamma$ ; having  $\delta_i = -1$  invariant, while the additional label ‘T’ denotes TRS protection. In the column denoted ‘Phase’ we introduce a convenient but imprecise shorthand notation.

the ‘ $\Gamma$ ’ phase, has  $\delta_\Gamma = -1$  at the  $\Gamma$ -point in the Brillouin zone and  $\delta_i = 1$  at all the other high-symmetry points. A crucial observation is that the distribution of signs of the Pfaffian,  $\delta_i$ , at the points  $\Gamma_i$ , and not only their product, encodes the additional topological structure. To show this, we first consider how the matrix of overlaps transforms under a lattice symmetry operation represented by a unitary operator  $U$

$$w_{mn}(\mathbf{k}) = \langle u_m(-\mathbf{k}) | \vartheta | u_n(\mathbf{k}) \rangle$$

$$= \langle u_m(-U\mathbf{k}) | U \vartheta U^\dagger | u_n(U\mathbf{k}) \rangle = w_{mn}(U\mathbf{k}) \quad (3)$$

As a consequence, when some of these high symmetry points are related by point-group symmetry of the lattice, their signs of the Pfaffian have to be equal. Therefore, it is sufficient to consider a subset,  $\Gamma_a$ , of representative, inequivalent high symmetry points that are also not related by any symmetry. This leads to the following rule that allows for the determination of all the topological phases given the space group and the corresponding high symmetry points,  $\Gamma_i$ : each phase is obtained by selecting a single representative high-symmetry point  $\Gamma_a$  and setting  $\delta_{\Gamma_a} = -1$ , which automatically sets  $\delta_{\Gamma_b} = -1$  at all the high-symmetry points  $\Gamma_b$  related by point group symmetry to  $\Gamma_a$ . Such phases are separated by a topological quantum phase transition that involves bulk bandgap closing, which changes the values of the  $\delta_i$ .

Let us illustrate this simple classification principle by an elementary example. We start with the  $\Gamma$  phase on a square lattice,  $\delta_\Gamma = -1$ , and  $\delta_X = \delta_Y = \delta_M = 1$ , where X, Y, and M are the TRI momenta in the Brillouin zone. By applying our rule, we immediately see that, besides the  $\Gamma$  phase, we obtain an ‘M’ phase with  $\delta_M = -1$ , and  $\delta_\Gamma = \delta_X = \delta_Y = 1$  (Table 1). This phase is disconnected from the  $\Gamma$  phase through a topological quantum phase transition with the bandgap closing at the X and the Y points. This phase is protected by TRS and is also susceptible to

dislocations<sup>27</sup>, and represents an example of a ‘translationally active’ phase. Furthermore, because the X and the Y points are related by a  $C_4$  rotation, there can exist a phase with  $\delta_X = \delta_Y = -1$ , and  $\delta_\Gamma = \delta_M = 1$ . The product of the  $\delta_i$  at all TRI momenta then yields the trivial  $Z_2$  invariant,  $\nu = 0$ . However,  $C_4$  rotational symmetry protects this phase, because it pins the band inversions at the X and Y points. This phase represents a ‘valley’ (or ‘crystalline’<sup>23</sup>) insulator—a phase which is trivial according to the ten-fold way but protected by the lattice symmetries. Indeed, this new phase, which we dub the ‘X–Y’ phase, is realized in an extension of the M–B model for a quantum spin Hall insulator with next-nearest neighbour hopping, as shown in Fig. 1, and responds nontrivially to dislocations; see Supplementary Information for the technical details. When  $C_4$  rotational symmetry is reduced to  $C_2$ , the X and Y points are no longer related by symmetry, and therefore the symmetry constraints on  $\delta_X$  and  $\delta_Y$  are no longer present. We then expect the X–Y phase to be unstable, and to yield instead nontrivial phases with  $\delta_X = -1$  or  $\delta_Y = -1$ , and  $\delta_i = 1$  at all other TRI momenta. Our calculations, indeed, confirm this within the M–B tight-binding model, as shown in Supplementary Section SA. In general, an even number of TRI momenta related by symmetry yield a valley phase, protected by crystal symmetry while having  $\nu = 0$ .

Let us now elaborate on the role of the space group of the underlying lattice in this classification, as this symmetry group defines the relation between the high-symmetry points. The difference in phases found on rectangular and rhombic lattices serves as a clear illustration. Both these lattices have  $D_2$  point-group symmetry, but different wallpaper groups (space groups in 2D). The rhombic case has two inequivalent TRI momenta related by point group symmetry and hence a valley phase, see Table 1 and Supplementary Section SA. On the other hand, in the rectangular case all  $D_2$  symmetry operations map any TRI momentum to its equivalent, thus no valley phase is possible. From Table 1 it can be seen that in 2D the phases, as related to space groups, cluster

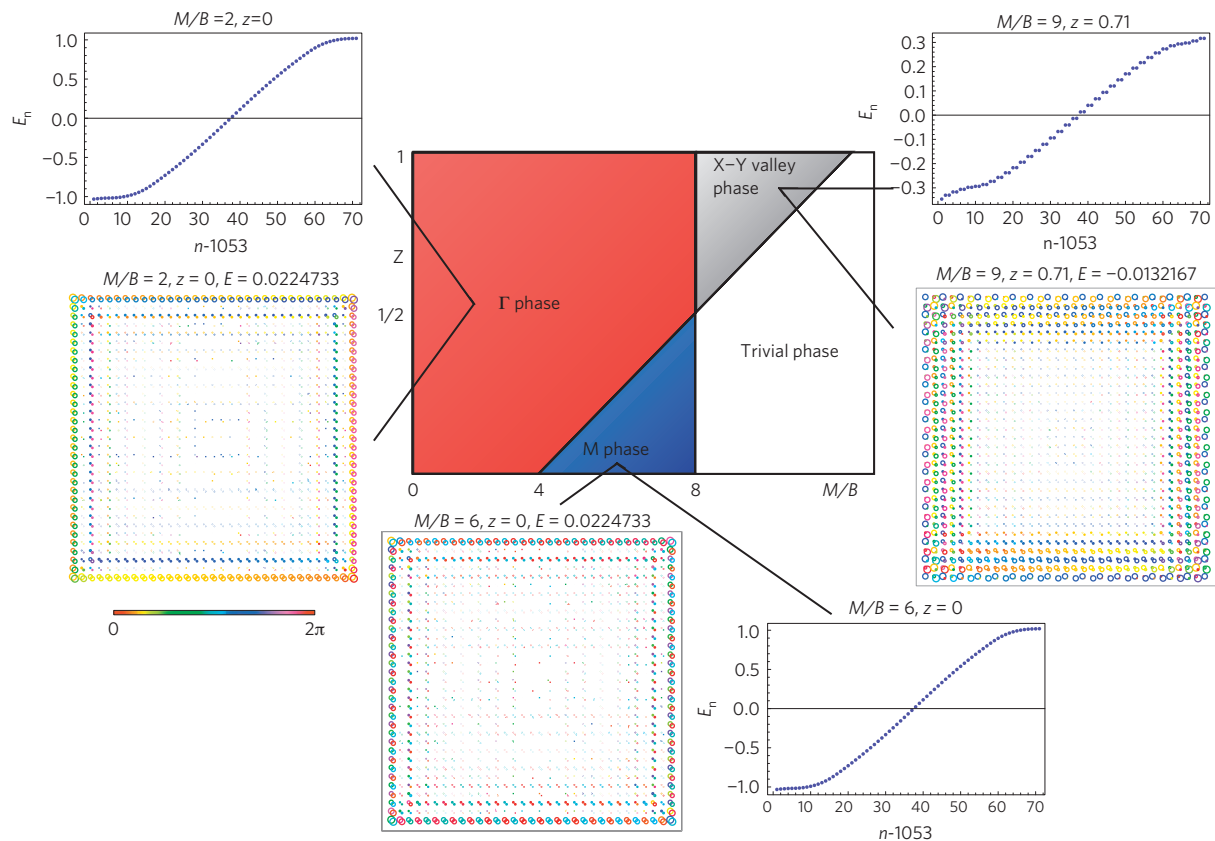


**Figure 1 | Phase diagram of the extended  $M$ - $B$  tight-binding model.** As function of the model parameters  $M/B$  and  $z = \tilde{B}/B$ , where  $B$  ( $\tilde{B}$ ) is the (next) nearest-neighbour hopping parameter and  $M$  the difference in on-site energies, the different distributions of  $\delta_i$  are obtained with the corresponding phases listed in Table 1; consult Supplementary Section SA for details.  $E_n$  is energy of the edge mode labelled by  $n$  in units of the nearest-neighbor hopping between  $s$ - and  $p$ -orbitals. Furthermore, the spectra of edge states per spin component are shown for the non-trivial phases, demonstrating that the valley  $X$ - $Y$  phase exhibits a pair of Kramers pairs of metallic edge states. The real space localization of these edge states is also presented, where the radii of the circles represent the magnitude of the wave function and the colours indicate the phases as shown on the left.

in Bravais lattice classes, with one exception: the hexagonal lattice. We will see that this clustering is less generic in 3D. In turn, the primitive Bravais hexagonal (triangular) lattice ( $p6mm$ ) is invariant under  $C_6$  rotational symmetry around a lattice site, as opposed to the non-primitive hexagonal lattice ( $p3m1$ ) realized in graphene. On the basis of our rule, we conclude that in the latter case only the  $\Gamma$  phase is possible, which is in fact realized in the Kane–Mele model<sup>28</sup>. In contrast, on the former lattice (triangular), the points  $K_+$  and  $K_-$  are related by a  $C_6$  symmetry and thus each of these points becomes TRI. The number of TRI momenta is increased, ultimately yielding a possibility of additional translationally active and valley phases, as shown in Table 1. These phases are realized within the  $M$ - $B$  tight-binding model (Supplementary Section SA), and their robustness against disorder is shown in Supplementary Section SB.

The above rule allows us to completely classify and index the topological phases: the last entry in Table 1. The set of Brillouin zone high-symmetry points  $\Gamma_i$  at which there is band inversion, that is,  $\delta_{\Gamma_i} = -1$ , is invariant under the operations of a subgroup of the lattice space group. This symmetry subgroup therefore protects and labels the topological phase. The other element in this indexing is the protection by TRS ( $T$ ), existing when  $Z_2$  invariant  $\nu = 1$ , giving, for instance,  $T$ - $p4mm$  as the  $\Gamma$  phase on the square lattice. When the protecting symmetries coincide between phases, we explicitly label  $\Gamma_i$  (lower index), as, for example, for  $T$ - $p2m_x$ ,  $T$ - $p2m_y$  and  $T$ - $p2m_M$  phases on the rectangular lattice. This leads to the list of topological phases in 2D presented in Table 1, which gives 18 distinct topological phases. As our general result, there are two additional broad classes of topological states protected by TRS or crystalline

symmetries, besides the class of states robust against general TRS perturbations ( $\Gamma$ -states): translationally active states protected both by TRS and lattice symmetry, responding to dislocations, and valley insulators which are trivial according to the ten-fold way but protected by space group symmetry and also susceptible to dislocations.

Our procedure can be applied in the same way in 3D, but it becomes more involved given the 230 space groups and the large number of high-symmetry points. We find at least 70 different phases (R–J. Slager, A. Mesaros, V. Juričić, J. Zaanen, manuscript in preparation). Here we will illustrate these matters for a number of simple crystal structures (Table 2) that include those of TBIs of present empirical relevance<sup>13–16</sup>. To illustrate matters, consider the primitive cubic lattice (Table 2) with the familiar eight TRI points (Fig. 2a). Crucially, the points ( $X, Y, Z$ ) are related by a three-fold rotation, as well as the points ( $X', Y', M$ ). Consequently, we obtain four TRS protected phases. We notice that this is quite different from the indexing procedure introduced by Moore and Balents<sup>5</sup>. For instance, our  $T$ - $pm\bar{3}m$  ( $\Gamma$ ) and  $T$ - $p\bar{3}(4)_R$  (R) phases correspond with their (1; 0, 0, 0) and (1; 1, 1, 1) indices, respectively. Their latter two indices would also correspond with the  $T$ - $p\bar{3}(4)_M$  and  $T$ - $p\bar{3}(4)_X$  phases, respectively. The other possibilities in their classification are either coincident with our four TBIs, or represent a 3D phase not protected by crystal symmetries due to implicit dimensional reduction (for example layered 3D lattice); Fig. 2a,b.

The power of the space group classification becomes further manifest for non-cubic lattices. Consider the 3D hexagonal lattice that consists of two hexagonal layers with the wallpaper group  $p6mm$  stacked on top of each other. The TRI momenta

**Table 2 | Topological phases predicted in 3D for some specific point group symmetries.**

Bravais lattice	PGS	SG	$\Gamma_i$	$\delta_i$	Index (phase)
Primitive cubic	$O_h$	$pm\bar{3}m$	$(\Gamma, R, X, M)$	$(-1, 1, 1, 1)$	$T-pm\bar{3}m (\Gamma)$
		$pn\bar{3}n$		$(1, -1, 1, 1)$	$T-p3(4)_R (R)$
		$pn\bar{3}m$		$(1, 1, -1, 1)$	$T-p3(4)_X (XYZ)$
		$pm\bar{3}n$		$(1, 1, 1, -1)$	$T-p3(4)_M (MX'Y')$
Hexagonal	$C_{6v}$	$p6mm$	$(\Gamma, M, A, L, K, H)$	$(-1, 1, 1, 1, 1, 1)$	$T-p6mm (\Gamma)$
		$p6cc$		$(1, -1, 1, 1, 1, 1)$	$T-p6_M (M)$
		$p6_3cm$		$(1, 1, -1, 1, 1, 1)$	$T-p6_A (A)$
		$p6_3mc$		$(1, 1, 1, -1, 1, 1)$	$T-p6_L (L)$
				$(-1, 1, 1, 1, 1, -1)$	$T-p6_{\Gamma H} (\Gamma H)$
				$(1, -1, 1, 1, 1, -1)$	$T-p6_{HM} (MH)$
				$(1, 1, -1, 1, -1, 1)$	$T-p6_{KA} (KA)$
				$(1, 1, 1, -1, -1, 1)$	$T-p6_{LK} (LK)$
Face centered cubic	$O_h$	$fm\bar{3}m$	$(\Gamma, X, L, U, W)$	$(-1, 1, 1, 1, 1, 1)$	$T-fm\bar{3}m (\Gamma)$
		$fm\bar{3}c$		$(1, -1, 1, 1, 1, 1)$	$T-f3(4) (X)$
		$fd\bar{3}m$		$(1, 1, -1, 1, 1, 1)$	$f3(4) (L\text{-valley})$
		$fd\bar{3}c$		$(1, 1, 1, -1, 1, 1)$	$f43_U (U\text{-valley})$
				$(1, 1, 1, 1, -1, 1)$	$f43_W (W\text{-valley})$
Rhombohedral	$D_{3d}$	$r\bar{3}m$	$(\Gamma, L, F, Z, P, K, B)$	$(-1, 1, 1, 1, 1, 1, 1)$	$T-r\bar{3}m (\Gamma)$
		$r\bar{3}c$		$(1, -1, 1, 1, 1, 1, 1)$	$T-r\bar{3}_L (L)$
				$(1, 1, -1, 1, 1, 1, 1)$	$T-r\bar{3}_F (F)$
				$(1, 1, 1, -1, 1, 1, 1)$	$T-r\bar{3}_Z (Z)$
				$(1, 1, 1, 1, -1, 1, 1)$	$r\bar{3}_P (P\text{-valley})$
				$(1, 1, 1, 1, 1, -1, 1)$	$r\bar{3}_K (K\text{-valley})$
				$(1, 1, 1, 1, 1, 1, -1)$	$r\bar{3}_B (B\text{-valley})$

Bravais lattices with same point-group symmetries have different space groups (SG). We point out that, in contrast to the 2D case, the phases do not cluster in Bravais lattice structures. For example, the four-fold rotational symmetry crucial for the  $f43_U$  and  $f43_W$  phases is not contained in every space group associated with the face-centred cubic lattice. As the  $\delta_i$  attain the same value at the points  $\Gamma_i$  related by lattice symmetry or a reciprocal lattice vector, only one representative is given from each set of such points. We note that the rhombohedral  $T-r\bar{3}_L$  phase is observed in  $Bi_{1-x}Sb_x$  (refs 13,14), whereas the  $T-r\bar{3}m$  phase is found in  $Bi_2Se_3$  (ref. 15) and  $Bi_2Te_3$  (ref. 16). Moreover, the  $fm\bar{3}m-f3(4)$  phase has recently been observed in SnTe (ref. 30), as well as in the Sn-doped compounds PbTe (ref. 31) and PbSe (ref. 32).

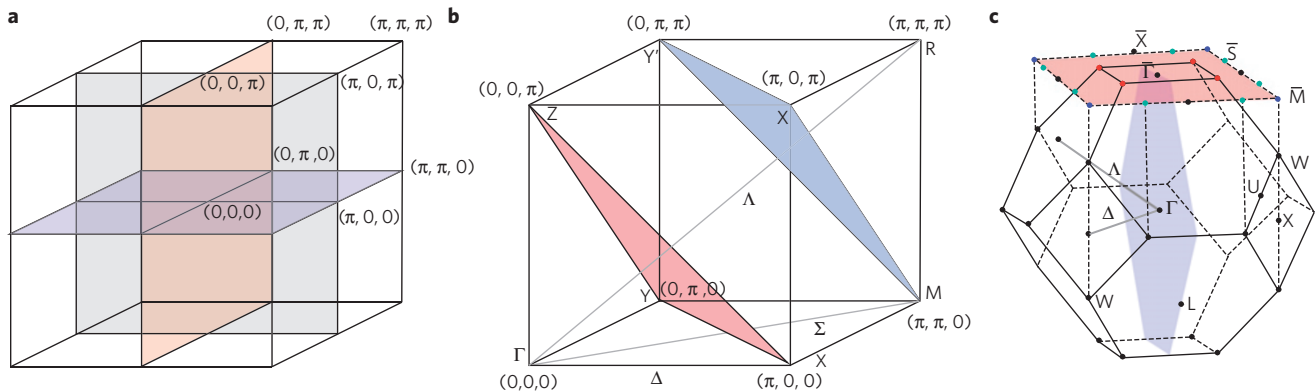


**Figure 2 | Illustration of the role of lattice symmetries in the classification of topological states. a**, The eight TR1 momenta in the Brillouin zone of the primitive cubic lattice. When only TRS is considered the sign of any quadruple of  $\delta_i$  values within a plane connecting them can be changed, leaving their product the same. As a result one obtains, in addition to the ‘strong’ invariant, three weak invariants corresponding to the orthogonal planes. **b**, The constraints on the  $\delta_i$  arising from the lattice symmetries. The high-symmetry axes  $\Delta$ ,  $\Lambda$  and  $\Sigma$  represent axes of four-, three- and two-fold rotations, respectively; these transform the TR1 points in the coloured planes into each other, and thus constrain the corresponding  $\delta_i$  to be equal. **c**, The Brillouin zone of the face-centred cubic lattice with high-symmetry points and a mirror plane that projects onto the  $\bar{\Gamma}-\bar{X}-\bar{\Gamma}$  line in the (001) plane. The W-valley phase features Dirac cones along  $\bar{\Gamma}-\bar{M}-\bar{\Gamma}$  and  $\bar{\Gamma}-\bar{S}-\bar{\Gamma}$  lines, but not along  $\bar{\Gamma}-\bar{X}-\bar{\Gamma}$  lines.

comprise two copies of the ones on the 2D hexagonal lattice, separated by a perpendicular translation. Accordingly, the phases can easily be obtained by considering the  $k_z = 0$  plane (Table 1), which contains the  $\Gamma$ , M and K points, and those of the other translated plane associated with the points A, L and H, respectively (Table 2). Consequently, there are eight TRS protected phases resulting from the combinations of a TRS protected

phase in one plane and a trivial or a valley configuration in the other plane. Additionally, there are two valley phases that are configurations with one plane featuring a valley phase and the other a trivial configuration. Notice that a potential double valley phase with a valley phase in each of the planes is not protected by 3D crystal symmetry and is therefore trivial. We again point out that the truly 3D valley phase is determined

by a 3D point group, namely, the one whose action cannot be reduced to the 2D case.

Most experimentally observed TBIs are of the  $\Gamma$  kind, such as  $\text{Bi}_2\text{Se}_3$  (ref. 15) and  $\text{Bi}_2\text{Te}_3$  (ref. 16), except for  $\text{Bi}_{1-x}\text{Sb}_x$ , where the 3D pursuit started<sup>13,14</sup>, which is  $r\bar{3}m - T - r\bar{3}_L$ . The theoretically predicted rocksalt actinides<sup>29</sup> are actually of the translationally active class  $fm\bar{3}m - T - f3(4)$ . SnTe, as well as Sn-doped compounds PbTe and PbSe, have the same space group, but the phase recently observed in these compounds has no TRS protection<sup>30–32</sup> and is a valley phase<sup>23</sup>. Let us inspect this phase in more detail. This phase turns out to be indexed as  $fm\bar{3}m - f3(4)$  (Table 2). The system has mirror planes in the momentum space formed by the  $\Gamma$  and any two of the L points, which thereby relate the remaining two L points by symmetry. As a result, a mirror-symmetric crystal cut along the  $\bar{\Gamma}-\bar{X}-\bar{\Gamma}$  line in the (001) surface features a pair of Dirac cones (a double Dirac cone), which is therefore also protected by the same symmetry<sup>24</sup>. Notice that we also predict valley phases at the W and the U points in the Brillouin zone protected by both the four-fold and the three-fold rotational symmetries, labelled by  $fm\bar{3}m - f43_W$  and  $fm\bar{3}m - f43_U$ , respectively. The W-phase originates from six inequivalent symmetry-related W-points in the Brillouin zone where a band inversion gives rise to a valley phase. Furthermore, in the same phase, the (001) surface features Dirac cones for the cut along the  $\bar{\Gamma}-\bar{M}-\bar{\Gamma}$  and  $\bar{\Gamma}-\bar{S}-\bar{\Gamma}$  lines, but not along the  $\bar{\Gamma}-\bar{X}-\bar{\Gamma}$  direction, as is the case in the  $fm\bar{3}m - f3(4)$  phase; see Fig. 2. Therefore, the detection of the Dirac cones in the  $\bar{\Gamma}-\bar{M}-\bar{\Gamma}$  and  $\bar{\Gamma}-\bar{S}-\bar{\Gamma}$  directions in angle-resolved photoemission spectroscopy (ARPES) experiments would be a clear signature of this valley phase.

Our complete classification scheme, based on the full 2D and 3D space groups, has as its most important consequence that it demonstrates the potential existence of at least seventy distinct topological phases of insulating matter. We therefore anticipate that our results will be a valuable guide in the future exploration of the landscape of topological quantum matter. In particular, besides being useful for prediction and characterization of TBIs, the role of the crystal lattice we uncovered might also have consequences for the topological states in the presence of interactions and superconducting order. Our findings should also help further understand the role of lattice defects and disorder in the physics of the topological states of matter.

Received 27 July 2012; accepted 19 November 2012;  
published online 16 December 2012

## References

- Hasan, M. Z. & Kane, C. L. Colloquium: Topological insulators. *Rev. Mod. Phys.* **82**, 3045–3067 (2010).
- Qi, X. L. & Zhang, S. C. Topological insulators and superconductors. *Rev. Mod. Phys.* **83**, 1057–1110 (2011).
- Thouless, D. J., Kohmoto, M., Nightingale, M. P. & den Nijs, M. Quantized Hall conductance in a two-dimensional periodic potential. *Phys. Rev. Lett.* **49**, 405–408 (1982).
- Kane, C. L. & Mele, E. J.  $Z_2$  topological order and the quantum spin Hall effect. *Phys. Rev. Lett.* **95**, 146802 (2005).
- Moore, J. E. & Balents, L. Topological invariants of time-reversal-invariant band structures. *Phys. Rev. B* **75**, 121306 (2007).
- Fu, L. & Kane, C. L. Time reversal polarization and a  $Z_2$  adiabatic spin pump. *Phys. Rev. B* **74**, 195312 (2006).
- Fu, L. & Kane, C. L. Topological insulators in three dimensions. *Phys. Rev. Lett.* **98**, 106803 (2007).
- Fu, L. & Kane, C. L. Superconducting proximity effect and Majorana fermions at the surface of a topological insulator. *Phys. Rev. Lett.* **100**, 096407 (2008).
- Li, R. D., Wang, J., Qi, X. L. & Zhang, S. C. Dynamical axion field in topological magnetic insulators. *Nature Phys.* **6**, 284–288 (2010).

- Bernevig, B. A., Hughes, T. L. & Zhang, S. C. Quantum spin Hall effect and topological phase transition in HgTe quantum wells. *Science* **314**, 1757–1761 (2006).
- Zhang, H. *et al.* Topological insulators in  $\text{Bi}_2\text{Se}_3$ ,  $\text{Bi}_2\text{Te}_3$  and  $\text{Sb}_2\text{Te}_3$  with a single Dirac cone on the surface. *Nature Phys.* **5**, 438–442 (2009).
- König, M. *et al.* Quantum spin Hall insulator state in HgTe quantum wells. *Science* **318**, 766–770 (2007).
- Hsieh, D. *et al.* A topological Dirac insulator in a quantum spin Hall phase. *Nature* **452**, 970–974 (2008).
- Hsieh, D. *et al.* Observation of unconventional quantum spin textures in topological insulators. *Science* **323**, 919–922 (2009).
- Xia, Y. *et al.* Observation of a large-gap topological-insulator class with a single Dirac cone on the surface. *Nature Phys.* **5**, 398–402 (2009).
- Chen, Y. L. *et al.* Experimental realization of a three-dimensional topological insulator,  $\text{Bi}_2\text{Te}_3$ . *Science* **325**, 178–181 (2009).
- Schnyder, A. P., Ryu, S., Furusaki, A. & Ludwig, A. W. W. Classification of topological insulators and superconductors in three spatial dimensions. *Phys. Rev. B* **78**, 195125 (2008).
- Ryu, S., Schnyder, A. P., Furusaki, A. & Ludwig, A. W. W. Topological insulators and superconductors: ten-fold way and dimensional hierarchy. *New J. Phys.* **12**, 065010 (2010).
- Kitaev, A. Periodic table for topological insulators and superconductors. *AIP Conf. Proc.* **1134**, 22–30 (2009).
- Ran, Y., Zhang, Y. & Vishwanath, A. One-dimensional topologically protected modes in topological insulators with lattice dislocations. *Nature Phys.* **5**, 298–303 (2009).
- Fu, L. & Kane, C. L. Topological insulators with inversion symmetry. *Phys. Rev. B* **76**, 045302 (2007).
- Teo, J. C. Y., Fu, L. & Kane, C. L. Surface states and topological invariants in three-dimensional topological insulators: Application to  $\text{Bi}_{1-x}\text{Sb}_x$ . *Phys. Rev. B* **78**, 045426 (2008).
- Fu, L. Topological crystalline insulators. *Phys. Rev. Lett.* **106**, 106802 (2011).
- Hsieh, T. H., Lin, H., Liu, J., Duan, W., Bansil, A. & Fu, L. Topological crystalline insulators in the SnTe material class. *Nature Commun.* **3**, 982 (2012).
- Hughes, T. L., Prodan, E. & Bernevig, B. A. Inversion-symmetric topological insulators. *Phys. Rev. B* **83**, 245132 (2011).
- Turner, A. M., Zhang, Y., Mong, R. S. K. & Vishwanath, A. Quantized response and topology of magnetic insulators with inversion symmetry. *Phys. Rev. B* **85**, 165120 (2012).
- Juričić, V., Mesáros, A., Slager, R.-J. & Zaenen, J. Universal probes of two-dimensional topological insulators: dislocation and  $\pi$  flux. *Phys. Rev. Lett.* **108**, 106403 (2012).
- Kane, C. L. & Mele, E. J. Quantum spin Hall effect in graphene. *Phys. Rev. Lett.* **95**, 226801 (2005).
- Zhang, X., Zhang, H., Wang, J., Felser, C. & Zhang, S. C. Actinide topological insulator materials with strong interaction. *Science* **335**, 1464–1466 (2012).
- Tanaka, Y. *et al.* Experimental realization of a topological crystalline insulator in SnTe. *Nature Phys.* **8**, 800–803 (2012).
- Xu, S. Y. *et al.* Observation of a topological crystalline insulator phase and topological phase transition in  $\text{Pb}_{1-x}\text{Sn}_x\text{Te}$ . *Nature Commun.* **3**, 1192 (2012).
- Dziawa, P. *et al.* Topological crystalline insulator states in  $\text{Pb}_{1-x}\text{Sn}_x\text{Se}$ . *Nature Mater.* **11**, 1023–1027 (2012).
- Dresselhaus, M. S., Dresselhaus, G. & Jorio, A. *Group Theory Application to the Physics of Condensed Matter* (Springer, 2008).

## Acknowledgements

This work is supported by the Dutch Foundation for Fundamental Research on Matter (FOM). V.J. acknowledges the support of the Netherlands Organization for Scientific Research (NWO).

## Author contributions

All authors contributed extensively to the work presented in this paper.

## Additional information

Supplementary information is available in the online version of the paper. Reprints and permissions information is available online at [www.nature.com/reprints](http://www.nature.com/reprints). Correspondence and requests for materials should be addressed to V.J.

## Competing financial interests

The authors declare no competing financial interests.